https://doi.org/10.5194/egusphere-2026-2925
Preprint. Discussion started: 30 June 2026
© Author(s) 2026. CC BY 4.0 License.

Thermospheric shock waves and lensing of light in the Barium Release, Optical and Radio rocket experiment

Thomas B. Leyser[1], Tima Sergienko[2], Yoshihiro Yokoyama[3], Tomoe Taki[2], and Urban Brändström[2]

[1]Swedish Institute of Space Physics, Uppsala, Sweden.
[2]Swedish Institute of Space Physics, Kiruna, Sweden.
[3]Department of Physics and Technology, UiT The Arctic University of Norway, Tromsø, Norway.

Correspondence: Thomas B. Leyser (thomas.leyser@irfu.se)

Abstract. The Barium Release, Optical and Radio (BROR) rocket experiment, launched from Esrange near Kiruna, Sweden, involved eight releases of barium at different altitudes in the thermosphere to study electric fields near small scale auroral structures. The barium was ejected into the thermosphere by the explosion-like combustion of ignited copper oxide thermite. Shock waves could be observed optically from the ground to follow the barium ejections when the rocket speed was supersonic, but not when it was subsonic. The shock waves are attributed to copper droplets that resulted from the thermite combustion and other particulate matter in the ejecta that traveled at supersonic speed. The observed deceleration of the shock waves can be explained by frictional drag together with gravity on copper droplets having a mean radius of about $1\ \mathrm{mm}$. The actual observation of the shock waves from the ground is attributed to scattering of sunlight on the particulate matter in the ejecta. Also, following the ejections at the highest speeds, optical lensing of sunlight reflected from the rocket itself was observed, in that the rocket appeared brighter just after the barium release than before the release.

1 Introduction

The BROR (Barium Release, Optical and Radio) rocket was launched from Esrange outside Kiruna, Sweden, at 18:23:00 UTC on 23 March 2023. The experiment involved eight barium releases during the one rocket flight, to study fine structure of aurora. The narrow launch window was determined by that the sun had set on the ground but not at about 100 km altitude and higher, so that the barium released in the thermosphere could be ionized by sunlight while twilight prevailed on the ground to enable observations of the emissions from the barium ions as well as aurora at optical wavelengths.

Experiments to eject barium vapor in the thermosphere by a thermite reaction started being used in the 1960s to research upper atmosphere and ionosphere phenomena. It was discovered that solar ultraviolet radiation ionized the barium which produced long-lasting barium ion clouds with resonance lines in the visible spectrum (e.g., Föppl et al., 1967), such that under twilight conditions on the ground the development of the clouds could be observed through cameras and be used to observe ionospheric and thermospheric properties. This became a useful tool to study fine structure of aurora (e.g., Wescott et al., 1969; Fahleson et al., 1971; Best and Hoffman, 1974).

The main purpose of the BROR experiment was to study electric fields in the vicinity of auroral structures. The motion of an ionized barium cloud is influenced by the electric fields which therefore could be estimated from the optically detectable cloud.

https://doi.org/10.5194/egusphere-2026-2925
Preprint. Discussion started: 30 June 2026
© Author(s) 2026. CC BY 4.0 License.

Initial results from the experiment have been published by Taki et al. (2026). In the present treatment, however, the focus is not on the barium clouds themselves, but on shock waves observed as a result of several of the barium ejections. No observations of shock waves in such barium release experiments have been discussed previously. However, Rosenberg and Best (1971) observed in a barium release experiment a ring expanding around the barium cloud, at a supersonic radial velocity of 1 $\mathrm{km/s}$ perpendicular to the rocket trajectory. As the ring was observed through scattered sunlight it was attributed to particulate matter.

Observations of shock waves in the thermosphere due to rocket transits at supersonic speeds have mainly been made through their effect on the ionospheric plasma. Depending on the cut and projection of the rocket bow shock waves the ionospheric disturbances were typically V-shaped (e.g., Kakinami et al., 2013; Lin et al., 2014; Yasyukevich et al., 2024; Li et al., 2025) or circularly shaped (Chou et al., 2018), where the latter were observed for a near vertical rocket trajectory. These observations of the effects of shock waves were made by using arrays of groundbased GNSS receivers to measure total electron content. The rockets were much more powerful and caused observable perturbations in a much larger altitude range, as well as larger latitudinal and longitudinal region, than the BROR rocket that is the focus in the present paper.

Whereas previous observations were on the ionospheric effects of atmospheric shock waves, we present here optical observations of shock waves in the thermosphere itself. In five of the eight barium ejections, at which the rocket had the highest speed and was supersonic, a wave front could be observed following the release. The fact that the waves could be observed only when the rocket was supersonic makes us interprete them as being shock waves. Images are shown from a camera located 246 km approximately to the east of the Esrange launch site, near Sodankylä, Finland, and from a camera approximately 34 km south-east of Esrange, near Vittangi, Sweden.

2 Observations

The BROR experiment involved eight barium ejections in the thermosphere between about 130 km and 250 km altitude, five on the upleg of the rocket trajectory and three on the downleg. The barium was contained in eight cylindrical canisters stored in the nose of the rocket, each with 2.0 kg of a mixture composed of barium (1.578 kg), strontium (0.048 kg) and copper oxide (CuO) thermite (0.374 kg). After the rocket launch, the nose cone was ejected and the barium was released by ignition of the thermite at pre-determined times during the rocket flight, one canister at the time. The release occurred in an explosive event in which the barium, strontium and remnants of the thermite combustion (which included droplets of molten copper) were ejected approximately in the direction of the rocket nose. Whereas the resulting atomic barium and strontium quickly decelerated in interaction with the ambient thermosphere, the barium that was not atomized and the remnants from the thermite combustion continued as a spray in the ejection directions. The velocity of the ejecta relative to the ambient thermosphere consisted of the ejection velocity relative to the rocket and the rocket velocity, and was supersonic or near sonic in all releases except in the fifth and the sixth.

Figure 1 shows the rocket speed (yellow) together with the sound speed (blue) versus altitude. The rocket speed decreased throughout the displayed altitude range, since the two engine stages separated from the rocket before the rocket reached 100 km. The altitudes of the eight releases together with the direction of the rocket (up or down) at the release are indicated on

https://doi.org/10.5194/egusphere-2026-2925
Preprint. Discussion started: 30 June 2026
© Author(s) 2026. CC BY 4.0 License.

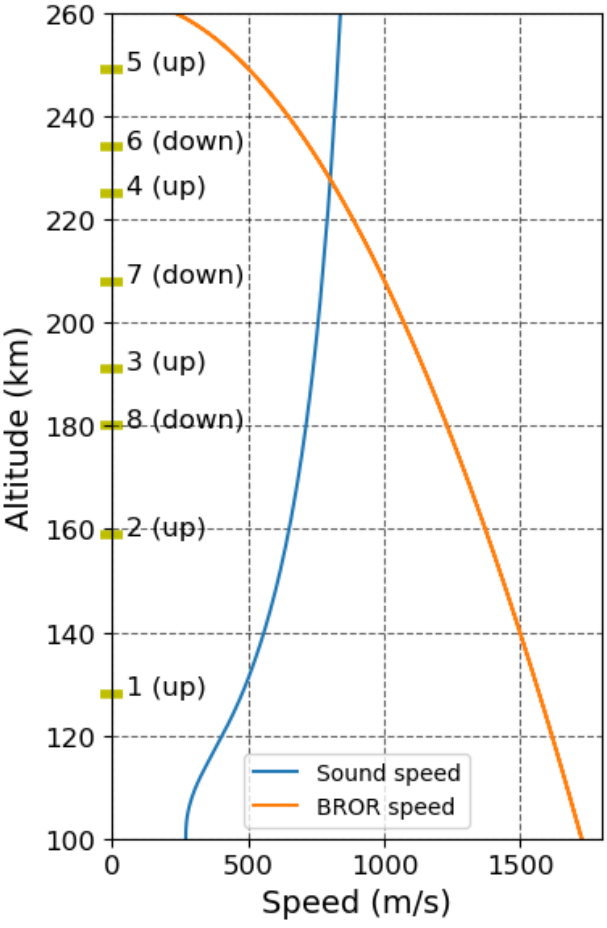

Figure 1. Altitude profiles of the speed of the BROR rocket and the sound speed in the thermosphere. The altitudes for the eight barium ejections as well as the direction of the rocket velocity (up or down) at the releases are indicated on the ordinate axis.

the ordinate axis. The rocket speed changed from a Mach number $M \gtrsim 4$ at 130 km altitude to $M \approx 1$ at about 230 km and $M < 1$ at higher altitudes. Shock waves following the barium ejections could be observed for the releases at the five lowest altitudes, at the first, second, third, seventh and eighth releases where the rocket speed was supersonic. A shock wave could possibly also be discerned following the fourth release, but only very weakly. As seen in Fig. 1, at the fourth release the rocket speed was close to sonic.

The sound speed c_s displayed in Fig. 1 was computed assuming an ideal gas: $c_s = (\gamma p/\rho)^{1/2}$, where we take $\gamma \approx 1.4$ as the heat capacity ratio for air, $p = n\,k_B\,T$ is the pressure (n, k_B, and T are the molecular number density, Boltzmann constant, and temperature, respectively), and ρ is the mass density of the ambient air. In view of that the dominating species in the altitude region of interest are N_2, O_2 and O, we take $n \approx n_{N_2} + n_{O_2} + n_O$. Altitude profiles for the values of n_{N_2}, n_{O_2}, n_O, T and ρ were taken from the MSIS90 model (Hedin, 1991; Emmert et al., 2021) for the date and local time of the experiment.

https://doi.org/10.5194/egusphere-2026-2925
Preprint. Discussion started: 30 June 2026
© Author(s) 2026. CC BY 4.0 License.

Figures 2–5 show images of shock waves from the first, second and eighth ejections, as observed from the Sodankylä camera site. These occurred at the three lowest altitudes where the rocket Mach number was the highest (Fig. 1). The images, originally in color, have been converted to grey-scale to bring forth irregularities in the shock waves. Figure 2 displays four images of the shock wave from the first ejection at an altitude of 128 km on the upleg of the rocket, with the images 4 s apart. The figure shows distances in the image plane, in elevation and azimuth as observed from the camera site. In Figs. 2a and 2b, both the sunlit barium cloud at the elevation distance in the image of -2.5 km and the upward propagating sunlit shock wave is seen. Figure 2b suggests a slightly conical shape of the shock wave. It should be kept in mind that the shock wave is viewed from obliquely below. Figures 2c and 2d display only the expanding shock wave. The images exhibit an irregular structure of the shock wave, which is particularly clear at the later times of the shock development (Figs. 2c and 2d).

Figure 3 is similar to Fig. 2, but for the second ejection at an altitude of 159 km. Both the barium cloud and the shock wave are larger than for the first release in Fig. 2. This is attributed to the lower ambient atmospheric pressure at the higher altitude of the second release compared to that of the first release. Similar to the case in Fig. 2, the sunlit shock wave exhibits inhomogeneities.

For a few seconds following the second ejection, striation-like structures can be seen between the shock wave and the barium cloud. An example is shown in Fig. 4 from 18:24:50 UTC and are indicated by the yellow arrows. Such structure can also be discerned in Fig. 3b from 18:24:51 UTC. We do not know what caused these striations, but presumably they are due to remnants of the explosive products that were ejected somewhat later than the main release.

Figure 5 displays the shock wave that followed the last ejection, on the downleg of the rocket trajectory at an altitude of 180 km. On the downleg, the rocket nose was still directed upward (the rocket body did not turn around at apogee) so that the barium with the remnants of the ignited thermite was ejected in that direction, approximately opposite to the rocket velocity. However, the speed of the ejecta (upward relative to the rocket) was much smaller than that of the rocket. Therefore, whereas the barium cloud quickly decelerated after release, the shock wave propagated downward and below the barium cloud that can be discerned near the upper center of the images in Fig. 5. Also, again the images exhibit irregularities in the shock wave.

Images like those in Figs. 2–5 were used to estimate the speed of the shock waves. Figure 6 illustrates the method by which this was done by displaying data from the second ejection, with distance and time from the point of release. As the geographic coordinates of the rocket trajectory versus time are known, each image pixel along the trajectory can be associated with geographic coordinates. Figure 6a depicts the light intensity (black) along the direction of the rocket velocity a few seconds after ejection with the background subtracted and a gaussian function fitted to the shock wave peak (purple). The maximum of the fitted gaussian is indicated by the blue circle and the shock front at half the maximum is indicated by a red star. Figure 6b shows the distance from the release point versus time after release, of the shock peak (blue dots) and front (red dots) as obtained from images one second apart, together with corresponding quadratic regression lines. The speed of the shock waves is then obtained from the time derivative of the regression lines. Since the speed of the shock front is higher than that of the shock wave peak, the shock wave widens with time as can also be seen from the images in Figs. 2–5.

Figures 7–9 display the obtained speeds of the shock waves versus time after ejection from the first, second and eighth ejection, respectively. The plots show the speed for the maximum (blue) of the scattered light intensity in the images and the

https://doi.org/10.5194/egusphere-2026-2925
Preprint. Discussion started: 30 June 2026
© Author(s) 2026. CC BY 4.0 License.

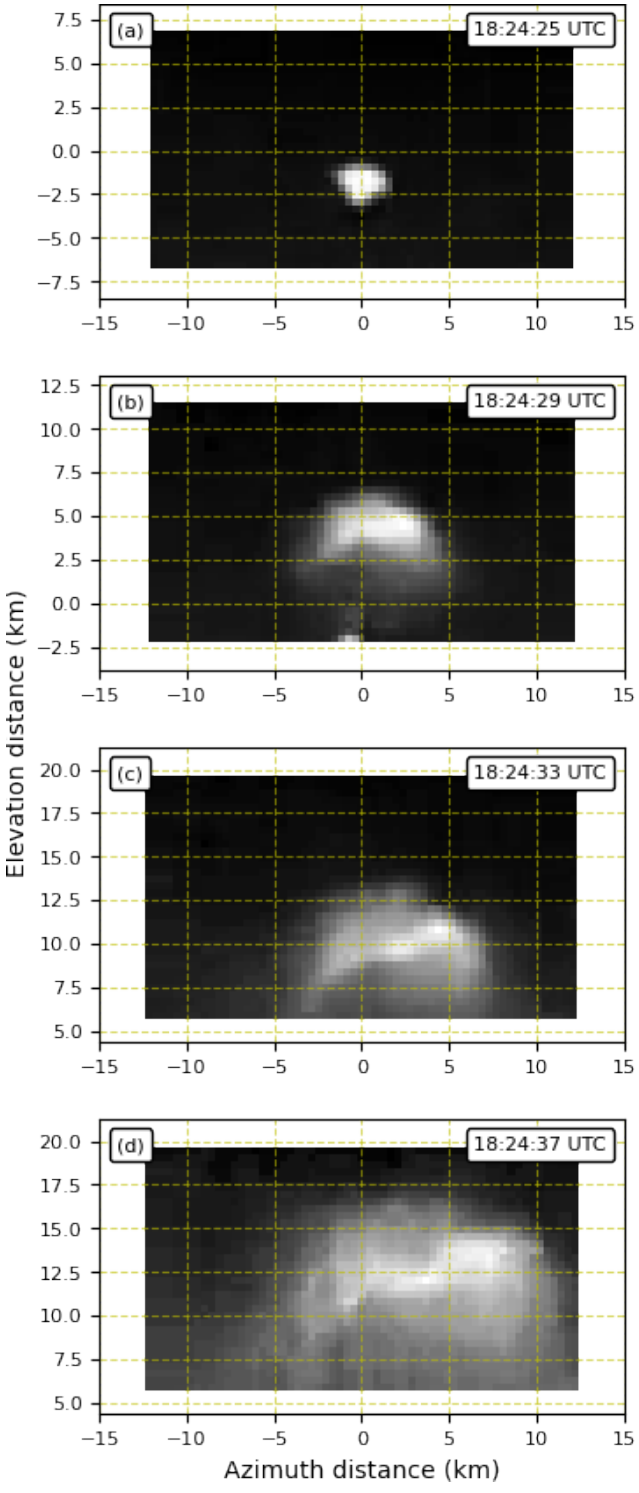

Figure 2. Images of the shock wave from the first barium ejection at 18:24:24 UTC (84 s after launch) on 23 March 2023, as observed from the Sodankylä camera site. (a) 18:24:25 UTC. (b) 18:24:29 UTC. (c) 18:24:33 UTC. (d) 18:24:37 UTC.

https://doi.org/10.5194/egusphere-2026-2925
Preprint. Discussion started: 30 June 2026
© Author(s) 2026. CC BY 4.0 License.

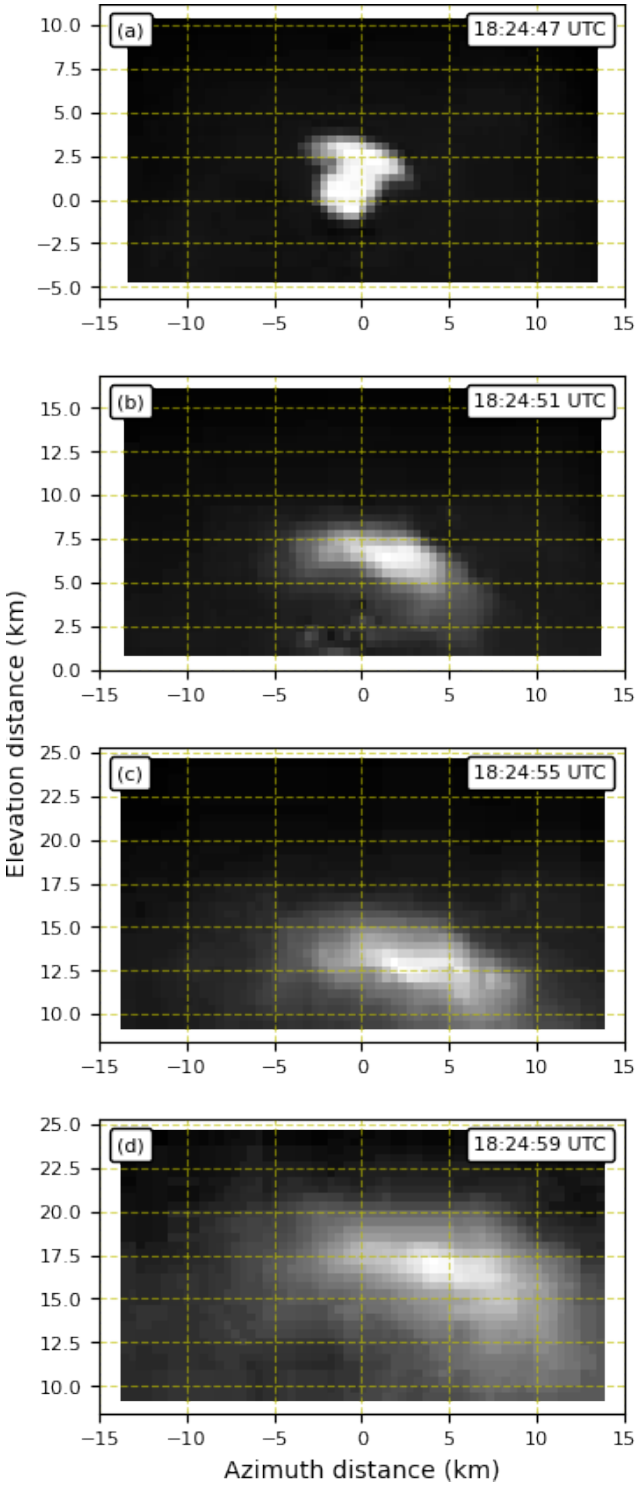

Figure 3. Images of the shock wave from the second barium ejection at 18:24:45 UTC (105 s after launch) on 23 March 2023, as observed from the Sodankylä camera site. (a) 18:24:47 UTC. (b) 18:24:51 UTC. (c) 18:24:55 UTC. (d) 18:24:59 UTC.

https://doi.org/10.5194/egusphere-2026-2925
Preprint. Discussion started: 30 June 2026
© Author(s) 2026. CC BY 4.0 License.

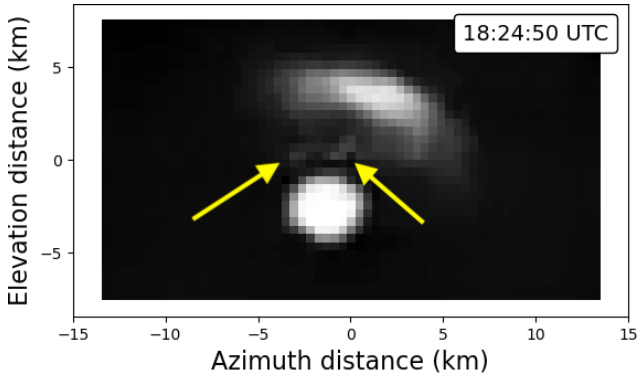

Figure 4. The same as for Fig. 3 but at 18:24:50 UTC, which shows striation-like features between the shock wave and the spherical barium cloud.

front (red) of the shock at an intensity a factor of 0.5 lower than the maximum. With a quadratic fit of the distance the shock waves travel with time (Fig. 6b), all speeds exhibit a linear dependence on time. For comparison, the speed of the rocket is shown as a dashed line. Also, the sound speeds c_{si} at the altitudes of the corresponding ejections (Fig. 1) are given by $c_{s1} \approx 0.48$ km/s, $c_{s2} \approx 0.65$ km/s and $c_{s8} \approx 0.73$ km/s. The maximum times after release for which the speeds are displayed in Figs. 7–9 are determined by that for larger times the estimate of the position of the shock waves in the images are too uncertain, since the images of the shock waves weaken with time (although data up to 20 s are displayed in Fig. 6b).

The largest speeds of the three ejections were obtained for the first ejection (Fig. 7) which occurred at the lowest altitude of all releases (Fig. 1). At the first ejection the rocket was on the upleg and decelerated due to gravity. The shock wave too traveled upward and faster than the rocket as the ignited thermite ejected the barium mixture and explosive products forward, approximately in the direction of the rocket velocity. It is seen that the shock wave exhibited higher deceleration than the rocket. The equations for the speed of the peak intensity u_1 (blue line in Fig. 7) and the shock front u_{1f} (red line in Fig. 7) versus time t after ejection are given by, respectively ($2 \le t \le 15$ s):

$$u_1 \approx 2027.58 - 55.22t \quad \text{m/s} \tag{1}$$

$$u_{1f} \approx 2179.59 - 46.52t \quad \text{m/s} \tag{2}$$

The shock maximum decelerated slightly faster than the shock front ($u_{1f} > u_1$) so that shock wave widened with time. Also, from Eq. (1) it is seen that the deceleration is $a_1 \approx -55.2$ m/s^2 which has a larger magnitude than that expected from gravity alone for which $g \approx 9.4$ m/s^2 at the thermospheric altitudes in question.

The situation is similar for the shock wave from the second ejection as shown in Fig. 8, but the deceleration was lower in this case although slightly higher than the deceleration of the rocket. The equations for the speed of the shock maximum (blue

https://doi.org/10.5194/egusphere-2026-2925
Preprint. Discussion started: 30 June 2026
© Author(s) 2026. CC BY 4.0 License.

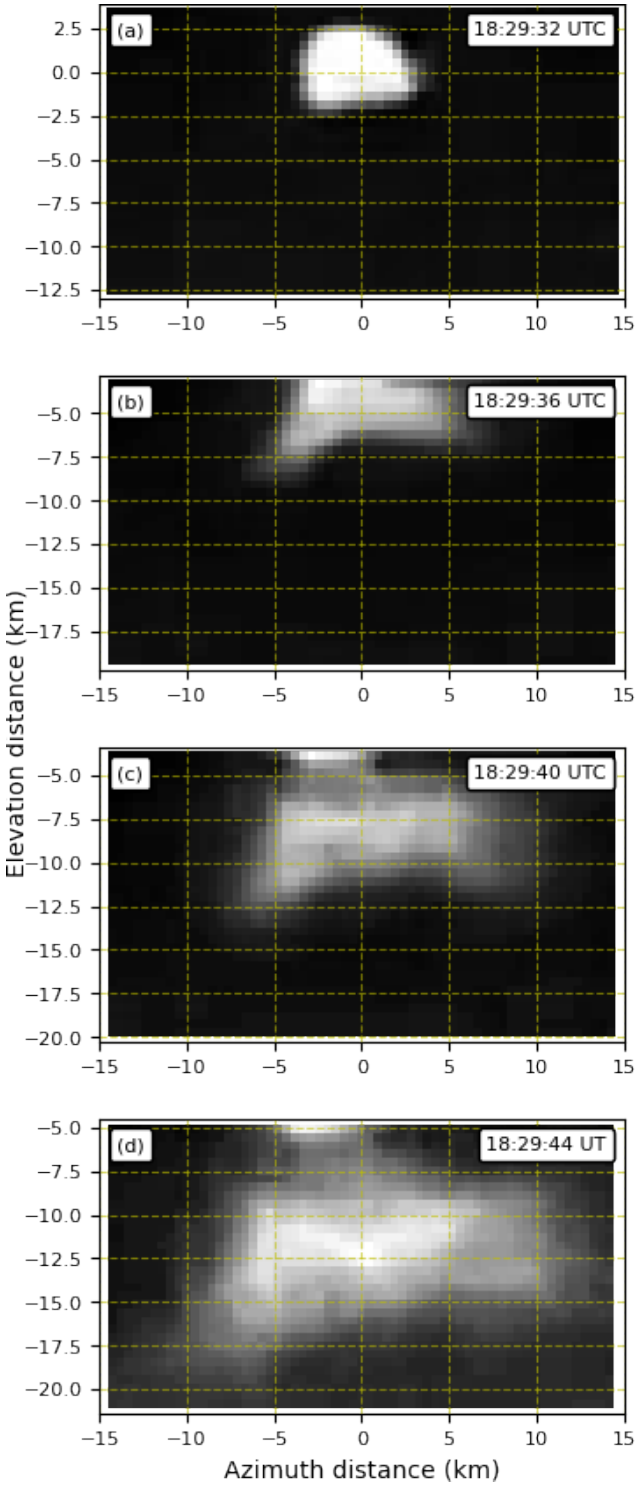

Figure 5. Images of the shock wave from the eighth barium ejection at 18:29:29 UTC (389 s after launch) on 23 March 2023, as observed from the Sodankylä camera site. (a) 18:29:32 UTC. (b) 18:29:36 UTC. (c) 18:29:40 UTC. (d) 18:29:44 UTC.

https://doi.org/10.5194/egusphere-2026-2925
Preprint. Discussion started: 30 June 2026
© Author(s) 2026. CC BY 4.0 License.

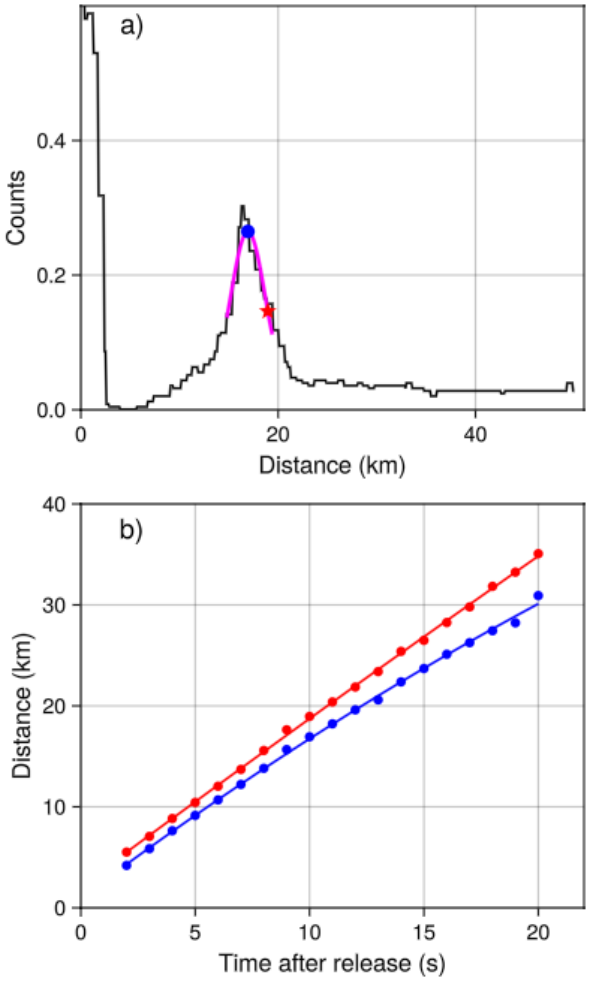

Figure 6. Description of the method used to obtain the speed of the shock waves with data from the second release. (a) Light intensity in the image versus distance along the direction of the rocket velocity a few seconds after the release (black) with the background light subtracted and a gaussian function fitted to the shock peak (purple). The maximum of the gaussian is indicated by a blue circle and the front at half the maximum is indicated by a red star. (b) Distance versus time after release of the shock maximum (blue dots) and front (red dots) together with corresponding quadratic regression lines.

https://doi.org/10.5194/egusphere-2026-2925
Preprint. Discussion started: 30 June 2026
© Author(s) 2026. CC BY 4.0 License.

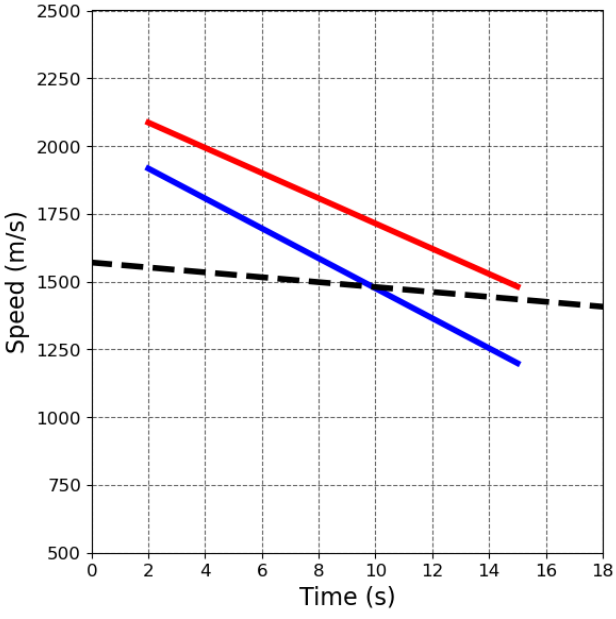

Figure 7. Speeds of the shock wave following the first ejection versus time t after release as obtained from a gaussian function fitted to the image intensity, for the intensity peak of the shock (blue) and the front (red). The rocket speed is shown as a dashed black line.

line in Fig. 8) and front (red line) are given by, respectively ($2 \leq t \leq 15$ s):

$$u_2 \approx 1757.25 - 30.62t \quad \mathrm{m/s} \tag{3}$$

$$u_{2\mathrm{f}} \approx 1780.40 - 16.65t \quad \mathrm{m/s} \tag{4}$$

Again we have $u_{2\mathrm{f}} > u_2$ so that the shock wave widened with time. From Eq. (3) it is seen that the deceleration is $a_2 \approx -30.6\ \mathrm{m/s^2}$ which has a larger magnitude than that expected from gravity alone.

For the first to the fifth releases, the explosive products were ejected forward and upward from the rocket. As the rocket nose still pointed upward on the downleg, the sixth to the eighth ejections too occurred upward while the rocket was falling downward with supersonic speed at the seventh and eighth releases (Fig. 1). Thus, whereas the explosive products were ejected upwards, the velocity of the associated shock wave relative to the ambient thermosphere was downward due to the high speed of the rocket. Figure 9 shows the shock wave speeds versus time from the eighth ejection. The shock wave maximum and front are both slower than the rocket, which is a result of that the barium mixture was ejected in the upward direction while the rocket was falling downward. For the eighth ejection the shock maximum decelerated with time whereas the shock front accelerated as given by the equations ($4 \leq t \leq 17$ s):

$$u_8 \approx 1024.53 - 9.11t \quad \mathrm{m/s} \tag{5}$$

https://doi.org/10.5194/egusphere-2026-2925
Preprint. Discussion started: 30 June 2026
© Author(s) 2026. CC BY 4.0 License.

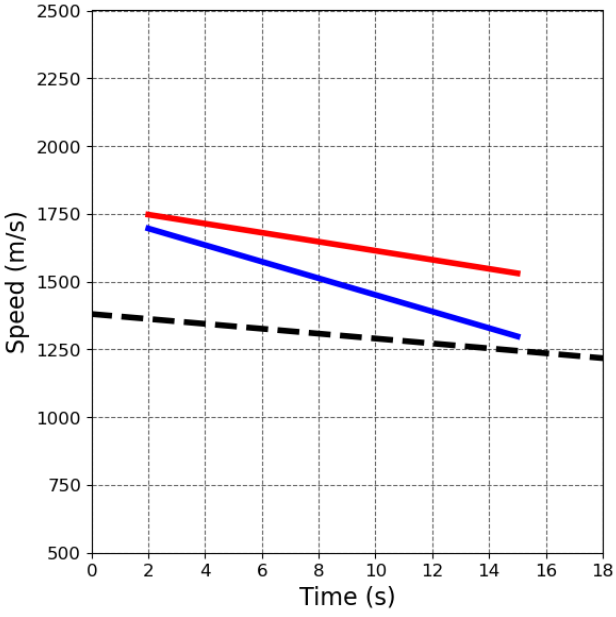

Figure 8. The same as Fig. 7 but for the shock wave following the second ejection.

$$u_{8\mathrm{f}} \approx 1039.18 + 5.89\,t \quad \mathrm{m/s} \tag{6}$$

In this case too we have $u_{8\mathrm{f}} > u_8$ so that the shock wave widens with time. From Eq. (5) we see that the deceleration of the shock maximum is $a_8 \approx -9.1\ \mathrm{m/s^2}$. Equation (6) shows that the acceleration of the shock front is $a_{8\mathrm{f}} \approx 5.9\ \mathrm{m/s^2}$, lower than g. Both a_8 and $a_{8\mathrm{f}}$ have magnitudes close to g which suggests that in this case gravity has a significant effect on the speed of the shock wave.

Another observation related to the shock waves concern reflected sunlight from the rocket itself. The rocket appeared brighter after an ejection compared to just before ejection. This lensing effect was only observed when the rocket speed was supersonic. Figure 10 displays two images from the Vittangi camera which had a higher resolution than the Sodankylä camera. The brighter backgrounds in Fig. 10 compared to those from the Sodankylä camera in Figs. 2–5 is attributed to that the latter was located more eastward, further into darkness than the twilight at the Vittangi camera.

Figure 10a is from 5 s before the first ejection and Fig. 10b is from 5 s after the ejection of the barium cloud that appears as the bright spot near the center of the image. The reflected light from the rocket can be seen as a small spot at the yellow arrow, in Fig. 10a before the ejection and in Fig. 10b as a brighter spot after the ejection. The reflected light from the rocket could be seen brightened for 10–15 s after the ejection. For comparison between the images, the red circles indicate the same three stars in Figs. 10a and 10b. Similar brightening of the sunlight reflected from the rocket could be seen following the second, third

https://doi.org/10.5194/egusphere-2026-2925
Preprint. Discussion started: 30 June 2026
© Author(s) 2026. CC BY 4.0 License.

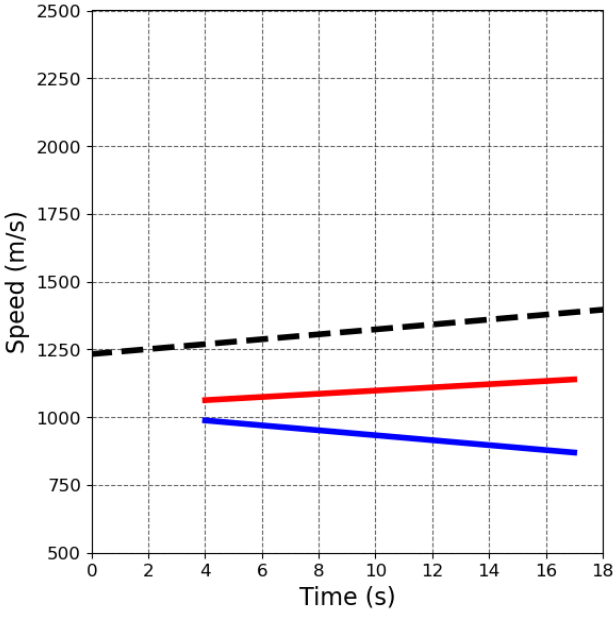

Figure 9. The same as Fig. 7 but for the shock wave following the eighth ejection versus time. Note that the velocities here are directed downward.

and fourth releases. The optical brightening could thus be observed for all ejections on the upleg at which the rocket speed was supersonic or sonic, but not when it was subsonic.

2.1 Discussion

The BROR rocket experiment involved eight barium releases at different altitudes in the thermosphere, five on the upleg of the rocket trajectory and three on the downleg. Following the explosive-like releases, waves could be observed in the five ejections at which the rocket speed was supersonic. Therefore we interpret them as shock waves. The barium was ejected and atomized by the explosive-like thermite combustion that produced droplets of copper, among other reaction products as well as barium that was not atomized. We consider the droplets and other remnants to be essentially sprayed into the ambient thermosphere.

As seen from Figs. 2–5, the shock waves appeared more blunt than cone-like. This is attributed to the angular spread of the sprayed ejecta, rather than from the interaction with the ambient thermosphere. The shock waves therefore appear to be bow shocks (curved detached shock waves) rather than shock cones (Mach cones) that would result from pointed solid objects such as the rocket itself. For example, a shock cone from a projectile at a Mach number $M = 3.0$, slightly smaller than the rocket speed at the first release (Fig. 1), would have a cone half-angle of $\theta = \arcsin(1/M) \approx 20^\circ$ which is much narrower than what might fit the shock wave in Fig. 2.

Shock waves are expected to have formed for both the rocket itself at its supersonic speed and the ejecta from the thermite combustion. However, the Mach cone from the rocket could not be observed. The effect of the density and pressure gradients

https://doi.org/10.5194/egusphere-2026-2925
Preprint. Discussion started: 30 June 2026
© Author(s) 2026. CC BY 4.0 License.

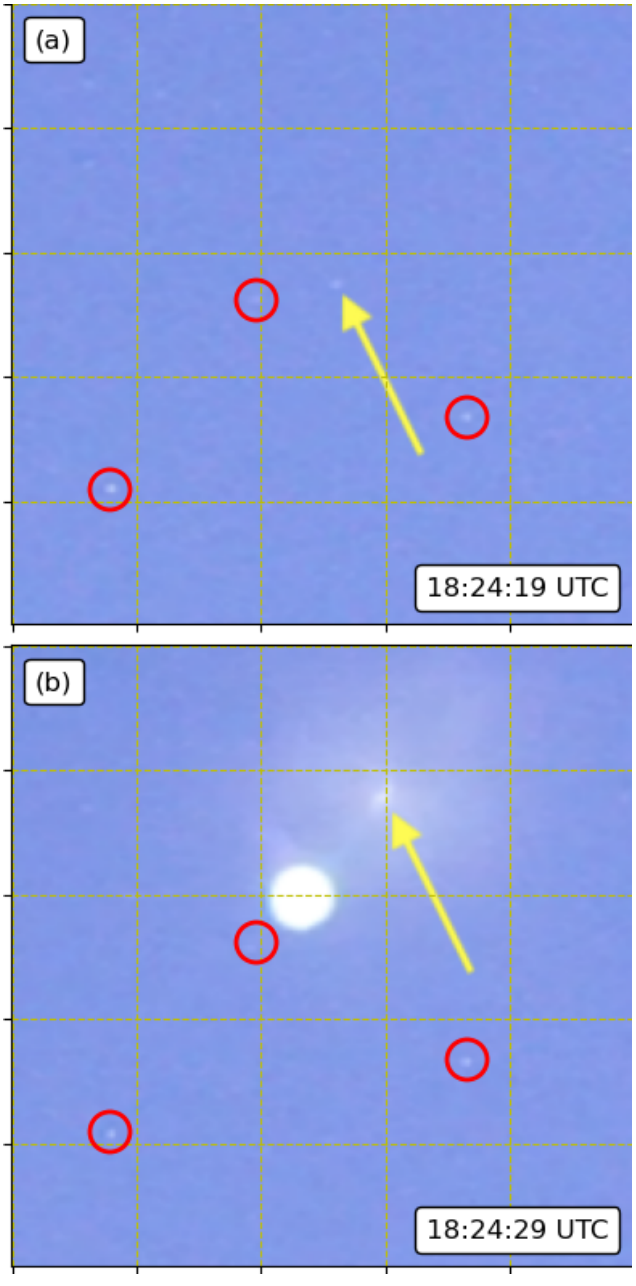

Figure 10. Images from the Vittangi camera site showing the rocket at the yellow arrow, (a) 5 s before the first ejection and (b) 5 s after the ejection. The bright barium cloud in (b) drifted (presumably with the neutral wind) downward to the left in the image after ejection, which is why it is not centered on the line between the rocket position in (a) and that in (b). In the panels the same three stars are encircled in red for comparison between the images.

https://doi.org/10.5194/egusphere-2026-2925
Preprint. Discussion started: 30 June 2026
© Author(s) 2026. CC BY 4.0 License.

associated with the shock cone on the scattering of sunlight in the thermosphere was too weak to be observed on the ground with the cameras used in the experiment. The observed shock waves were instead related to the barium ejections. As the ejecta included macroscopic particles much larger than the molecules of the thermospheric air, also particulate barium that had not been atomized, we attribute the observed shock waves to sunlight scattered off the copper droplets, particulate barium and other macroscopic reaction products in the supersonic flow of the ambient thermosphere.

Previous observations of sprays of droplets associated with shock waves have been made in the context of supersonic fuel sprays (e.g., MacPhee et al., 2002; Jia et al., 2016; Wang et al., 2017). For example, the fuel economy of diesel engines depends on fuel spray atomization and fuel-air mixing, and increasing injection pressure may increase performance.

The shock waves from the first, second and eighth barium releases were studied in detail (Figs. 2–5). The shock waves from the first and second releases initially had a higher speed than the rocket which is consistent with that the barium and remnants of the thermite combustion were ejected approximately in the direction of the rocket velocity. At the eighth release, the explosive products were ejected approximately in the direction opposite to the rocket velocity, but with the velocity relative to the thermosphere still directed downward, so that the speed of the shock was lower than that of the rocket.

The shock waves following the first, second and eighth releases decelerated approximately linearly with time, as shown in Figs. 7–9. We attribute this deceleration to gravity and frictional drag on the macroscopic ejecta due to the viscosity of the thermosphere. For the eighth release, the shock wave propagated downward so that the thermospheric wind came from below and interacted with the shock wave with higher pressure from below, despite that the thermite reaction products had been ejected upward. To analyze the speed of the shock waves, we assume for simplicity that the ejecta are mainly small spheres of molten copper and we consider only a single mean droplet in the spray moving through the air. The force acting on one sphere along its trajectory is $F = F_\mathrm{f} + F_\mathrm{g}$, where F_f and F_g are the frictional and gravitational forces, respectively.

The frictional force on a small sphere moving with the speed u through a viscous fluid at very small Reynolds numbers (to be checked below) is given by Stokes' law (e.g., Landau and Lifshitz, 1989):

$$F_\mathrm{f} = -6\pi\mu\, r\, u, \tag{7}$$

where μ is the dynamic viscosity and r is the radius of the sphere. This drag force is directed opposite to the velocity of the object. The viscosity is related to the temperature T by Sutherland's law:

$$\mu = \mu_\mathrm{ref} \left(\frac{T}{T_\mathrm{ref}} \right)^{3/2} \frac{T_\mathrm{ref} + S}{T + S}, \tag{8}$$

where for air $\mu_\mathrm{ref} = 1.716 \times 10^{-5}$ kg/m/s at the reference temperature $T_\mathrm{ref} = 273$ K, and the Sutherland constant $S = 111$ K (White, 1991). Taking the same temperature profile as for the computed sound speed in Fig. 1, we obtain the viscosity at the altitude of the first release (128 km), $\mu_1 \approx 2.70 \times 10^{-5}$ kg/m/s, at the second release (159 km), $\mu_2 \approx 3.79 \times 10^{-5}$ kg/m/s, and at the eighth release (180 km), $\mu_8 \approx 4.16 \times 10^{-5}$ kg/m/s. As T increases with altitude in the thermosphere, $\mu_1 < \mu_2 < \mu_8$.

For the gravitational force component on the sphere along its trajectory, we assume that the sphere is ejected approximately in the direction of the rocket velocity at the time of release for the first and second releases, and opposite to the rocket velocity for the eighth release. In reality the ejection occured around an angle of the rocket nose which itself stayed in approximately

https://doi.org/10.5194/egusphere-2026-2925
Preprint. Discussion started: 30 June 2026
© Author(s) 2026. CC BY 4.0 License.

the same direction throughout the rocket trajectory and was at an angle to the rocket velocity that changed along the trajectory. However, as discussed below, the speed of the ejecta relative to the rocket was much smaller than that of the rocket itself, which is therefore neglected.

With the rocket velocity at an angle $\alpha = \alpha_i$ to the upward vertical (for release $i = 1$, 2, 8), the gravitational force component in the direction of the rocket velocity is given by

$$F_{\rm g} = -mg\cos\alpha, \tag{9}$$

where m is the mass of the sphere, and for the first, second and eighth releases the gravitational acceleration is $g \approx 9.4\ {\rm m/s^2}$ at the altitudes in question, $\alpha_1 \approx 5.5°$, $\alpha_2 \approx 5.7°$ and $\alpha_8 \approx 160.6°$, respectively.

With $F = m\,du/dt$, Eqs. (7) and (9) give the differential equation

$$m\frac{du}{dt} = -6\pi\mu r\,u - mg\cos\alpha \tag{10}$$

which is solved by the following time dependence of the speed:

$$u(t) = \left(u_0 + \frac{mg\cos\alpha}{6\pi\mu r}\right)\exp\left(-6\pi\mu\frac{r}{m}t\right) - \frac{mg\cos\alpha}{6\pi\mu r}, \tag{11}$$

where t is the time after release and $u_0 = u(t=0)$. Expanding this expression with respect to t, we see that the time dependence of $u(t)$ is approximately linear for sufficiently small t, as also suggested by the observations in Figs. 7–9:

$$u(t) \approx u_0 - \left(6\pi\mu\frac{r}{m}u_0 + g\cos\alpha\right)t. \tag{12}$$

This equation can be compared to the experimentally determined speeds of the maximum part of the shock waves in Eqs. (1), (3) and (5), which are of the form $u_i \approx u_{0i} + a_i t$. From this the radius r of the sphere can be determined.

Assuming that the ejected explosive remnants of the thermite reaction are spheres of liquid copper, the mass of one sphere is $m = (4\pi r^3/3)\rho_{\rm Cu}$, where $\rho_{\rm Cu} \approx 8\,100\ {\rm kg/m^3}$ is the mass density of molten copper. The mean radius of the copper droplets needed to account for the observed deceleration of the main part of the shock wave from release i, is then obtained as

$$r_i \approx \left[\frac{9\mu_i u_{0i}}{2\rho_{\rm Cu}(-a_i - g\cos\alpha_i)}\right]^{1/2} \tag{13}$$

For the first ejection we have from Eq. (1), $u_{01} \approx 2027.58\ {\rm m/s}$ and $a_1 \approx -55.22\ {\rm m/s^2}$, which with $\alpha_1 \approx 5.5°$ and $\mu_1 \approx 2.70 \times 10^{-5}\ {\rm kg/m/s}$, gives $r_1 \approx 0.8\ \ {\rm mm}$. For the second release, Eq. (3) gives $u_{02} \approx 1757.25\ {\rm m/s}$ and $a_1 \approx -30.62\ {\rm m/s^2}$, which with $\alpha_2 \approx 5.7°$ and $\mu_2 \approx 3.79 \times 10^{-5}\ {\rm kg/m/s}$, gives $r_2 \approx 1.3\ \ {\rm mm}$. For the eighth release, Eq. (5) gives $u_{08} \approx 1024.53\ {\rm m/s}$ and $a_1 \approx -9.11\ {\rm m/s^2}$, which with $\alpha_8 \approx 160.6°$ and $\mu_8 \approx 4.16 \times 10^{-5}\ {\rm kg/m/s}$, gives $r_8 \approx 1.1\ \ {\rm mm}$. Thus, we obtain a mean radius of the copper droplets for the first, second and eighth releases of about $r \sim 1\ {\rm mm}$.

It may be noted that the thermite mixture before ignition had a particle size of $-200\ {\rm mesh}$, which corresponds to a size of about 75 μm and less. The upper limit of 75 μm is one order of magnitude smaller than the obtained mean radius of the copper droplets derived from the deceleration of the main part of the shock waves due to viscous drag and gravity.

https://doi.org/10.5194/egusphere-2026-2925
Preprint. Discussion started: 30 June 2026
© Author(s) 2026. CC BY 4.0 License.

Figure 9 for the eighth ejection shows that whereas the main part of the shock wave decelerated with time, as discussed above, the shock front accelerated at a rate slightly lower than the rocket. Above a mean radius of the droplets was considered. However, it is expected that a spray contains droplets with a range of sizes that are affected differently by viscous drag. This could account for some of the observed widening of the shock wave with time. Possibly, the accelerating shock front following the eighth ejection is due to larger droplets than the main part of the shock, which are less affected by frictional drag of the thermosphere and more controlled by gravity. The situation may be similar for the shock wave following the second ejection (Fig. 8), for which the shock front decelerated close to but slightly faster than the rocket while the main part of the shock decelerated faster than the front. This also indicates that viscous drag at the shock front was slightly larger than for the rocket.

To check our assumption of a low Reynolds number and dominance of viscous drag on the copper droplets, we take parameter values for the first and eighth releases. The Reynolds number is given by

$$Re = \frac{\rho u L}{\mu}, \tag{14}$$

where ρ is the thermospheric mass density at the ejection altitude and L is the characteristic length which is taken to be the mean diameter of the copper droplets. For the first release, with $\rho = \rho_1 \approx 5.93 \times 10^{-9}$ kg/m^3, taking the maximum speed in Eq. (1), $u = u_{01} \approx 2.03 \times 10^3$ m/s, $L = L_1 \approx 2 \times r_1 \approx 1.6 \times 10^{-3}$ m and $\mu = \mu_1$, we get $Re_1 \approx 7.1 \times 10^{-4}$. For the eighth release, $\rho = \rho_8 \approx 6.6 \times 10^{-10}$ kg/m^3, taking the maximum speed in Eq. (5), $u = u_{08} \approx 1.02 \times 10^3$ m/s, $L = L_8 \approx 2 \times r_8 \approx 2.2 \times 10^{-3}$ m and $\mu = \mu_8$, we get $Re_8 \approx 5.2 \times 10^{-5}$. As Re_1, $Re_8 \ll 1$, viscous forces dominate over inertial forces. And as $Re \ll 1$, the inhomogeneities in the shock waves seen in the images in Figs. 2–5 likely reflect corresponding inhomogeneities in the ejected explosive products, rather than turbulence in the interaction with the ambient thermosphere.

Another measure of the importance of viscosity and surface tension relative to inertial forces in determining the droplet size in a spray is given by the Ohnesorge number:

$$Oh = \frac{\mu}{\sqrt{\rho \sigma L}}, \tag{15}$$

where $\sigma = \sigma_{\mathrm{Cu}} \approx 1.32$ N/m is the surface tension of liquid copper near the melting point. With the parameters for the altitude of the first release, we have $\mu = \mu_1$, $\rho = \rho_1$ and $L = L_1$, we obtain $Oh_1 \approx 7.6$. At the altitude for the eighth release, $\mu = \mu_8$, $\rho = \rho_8$ and $L = L_8$, we obtain $Oh_8 \approx 30.0$. For both altitude regions, Oh_1, $Oh_8 > 1$, which means that viscous effects dominate over inertial forces.

From Eqs. (1), (3) and (5) we can obtain an estimate of the difference between the approximate speed of the shock wave, u_i, and the rocket, $u_{\mathrm{R}i}$, at the time of release $t = 0$ s. For the first release, $\Delta u_1 \equiv u_1(0) - u_{\mathrm{R1}} \approx 2.03 - 1.55 \approx 0.48$ km/s, and for the second release, $\Delta u_2 \equiv u_2(0) - u_{\mathrm{R2}} \approx 1.76 - 1.40 \approx 0.36$ km/s. For the eighth release, $\Delta u_8 \equiv u_8(0) - u_{\mathrm{R8}} \approx 1.02 - 1.25 \approx -0.23$ km/s. We have $\Delta u_1 > \Delta u_2 > |\Delta u_8|$ and interpret these speeds as the speeds relative to the rocket at which the reaction products of the thermite combustion were ejected into the ambient thermosphere. In all cases this speed was much smaller than that of the rocket. With the sound speeds at the release altitudes, $c_{\mathrm{s}1} \approx 0.48$ km/s, $c_{\mathrm{s}2} \approx 0.65$ km/s and $c_{\mathrm{s}8} \approx 0.73$ km/s (Fig. 1), the speed of the ejecta relative to the rocket was near sonic at the first release ($\Delta u_1 \approx c_{\mathrm{s}1}$) and subsonic at the second ($\Delta u_2 < c_{\mathrm{s}2}$) and eighth releases ($|\Delta u_8| < c_{\mathrm{s}8}$). We do not know why the ejection speed would decrease

https://doi.org/10.5194/egusphere-2026-2925
Preprint. Discussion started: 30 June 2026
© Author(s) 2026. CC BY 4.0 License.

with increasing altitude. In a test of the thermite combustion on the ground, where the air density and pressure are much higher than in the thermosphere, the speed of the ejecta was subsonic so that no blast wave was created. A consequence of that the shock speed was larger than the rocket speed for the first release, was that the shock wave from the second release propagated in the wake of the shock wave from the first release. Similarly, the shock wave from the third release propagated in the wake of that from the second release. For the eighth release, however, the shock wave instead propagated in the wake of the rocket.

Shock waves in air, such as from supersonic aircraft and rockets, can cause distortions in optical beams that cross the supersonic flows. Shock waves come with sharp gradients in air density and pressure which induce corresponding inhomogeneities in the refractive index and thus the propagation of light. The associated refraction of light has often been used to visualize shock waves by schlieren methods (e.g., Merzkirch, 1987). As optical beams do not not themselves introduce perturbations in the fluid flows, optical methods have been used extensively to investigate the turbulence of supersonic flows (e.g., Merzkirch, 1987; Banakh et al., 2007; Settles and Hargather, 2017; Wang et al., 2023).

In the BROR experiment, the rocket could be seen optically with the Vittangi camera throughout its trajectory in the sunlit thermosphere. Figure 10 shows an example of the rocket appearing brighter after a barium ejection compared to before the release. This optical lensing was only observed when the rocket speed was supersonic. Since the lensing followed the ejection, it is attributed to focussing by the shock wave from the ejecta as the rocket on its upleg propagated in the wake behind the shock wave. The density and pressure in the shock wake region are higher than in the unperturbed thermosphere in front of the shock wave, as given by the Rankine-Hugoniot relations (e.g., Landau and Lifshitz, 1989). The increased density and pressure increase the refractive index of the thermospheric air. With the rocket inside the wake region of increased refractive index, sunlight reflected from the rocket propagates in a region of decreasing refractive index out from the wake. This creates a gradient-index lens-like effect that could focus the reflected sunlight such that the rocket appeared brighter when observed from the ground.

The observed lensing effect was the strongest following the first ejection (Fig. 10), which occurred at the lowest altitude where both the Mach numbers of the rocket (Fig. 1) and shock wave were the highest. At the ejections at increasing altitudes lensing weakened. This can be understood by that with the decreasing Mach number of the rocket at increasing altitudes (Fig. 1), the perturbations of the refractive index from the shock waves would also decrease, and correspondingly also the refraction and focussing of sunlight reflected from the rocket.

3 Conclusions

The BROR rocket experiment involved eight releases of barium at different thermospheric altitudes to study electric fields in the vicinity of small-scale auroral structures. The barium was ejected by the explosive-like reaction of ignited copper oxide thermite that atomized part of the barium. This resulted in long-lasting barium clouds in the thermosphere that were ionized by sunlight, thereby being susceptible to electric fields near auroral structures. As the barium ions have resonance lines in the visible spectrum, cameras on the ground could track the motion of the clouds.

https://doi.org/10.5194/egusphere-2026-2925
Preprint. Discussion started: 30 June 2026
© Author(s) 2026. CC BY 4.0 License.

When the rocket speed was supersonic the barium ejections were followed by shock waves, as observed at optical wavelengths by cameras. The explosive-like thermite combustion produced, in addition to the atomized barium, also droplets of copper, particulate barium that had not been atomized and other macroscopic remnants. These products were sprayed into the thermosphere, forming bow shocks at the supersonic speeds. The observed shock waves are attributed to sunlight that scattered off the sprayed copper drops and other macroscopic particles. However, the thermospheric shock wave from the rocket itself was not observed.

The shock waves from the first, second and eighth ejections were studied in some detail. The speed of the shock waves could be determined up to about 15 s after the releases. During this time interval the speed of the maximum of the shock waves decreased linearly with time. This constant deceleration is attributed to gravity and frictional drag on the copper droplets propagating in the thermosphere. To account for the observed deceleration the droplets would need to have a mean radius of approximately 1 mm.

Sunlight scattered off the BROR rocket enabled it to be observed optically by cameras throughout its trajectory in the thermosphere. For a few seconds following the releases at the highest rocket speeds, the rocket appeared brighter than before the release. This optical lensing was observed on the upleg as long as the rocket speed was supersonic, which relates it to refractive index perturbations by the shock waves. Since the lensing followed the ejections and the rocket propagated in the wake of the shock wave, it is tentatively attributed to focussing of scattered sunlight by the wake behind the shock waves from the ejecta. Thus, sunlight was scattered off the supersonic macroscopic drops and particles of the ejecta which made the shock waves visible, as well as focussed and refracted by perturbations in the refractive index caused by the shock waves.

Data availability. The video from the Sodankylä site is available via the link https://www.youtube.com/watch?v=GUc5_ FtI7JM . The video from the Vittangi site is available via the link https://cloud.irf.se/s/gQqBJxkte4bFNC5 .

Author contributions. TL initiated the study, analyzed the data and wrote the paper. TS was the principal investigator of the BROR experiment, contributed to the data analysis and writing. YY operated the Vittangi camera and contributed to the writing. TT contributed to the data analysis and contributed to the writing. UB contributed to the organization of the experiment and operated cameras.

Competing interests. The contact author has declared that none of the authors has any competing interests.

Acknowledgements. The authors gratefully acknowledge Samuli Korvanen of Starlapland, Finland, for providing the video from near Sodankylä. The BROR project was made possible with the cooperation and assistance of the Swedish Institute of Space Physics, the Department of Physics and Astronomy of Clemson University, SSC Space, and the Mobile Rocket Base of the German Aerospace Center. We express special gratitude to Krister Sjölander (SSC Space), who played a crucial role in the design and manufacture of the payload, and to Miguel

https://doi.org/10.5194/egusphere-2026-2925
Preprint. Discussion started: 30 June 2026
© Author(s) 2026. CC BY 4.0 License.

Larsen (Clemson University) for sharing his experience in conducting rocket experiments for chemical release in the upper atmosphere. The BROR experiment was supported by the Swedish National Space Agency with the grant 2024-00232.

https://doi.org/10.5194/egusphere-2026-2925
Preprint. Discussion started: 30 June 2026
© Author(s) 2026. CC BY 4.0 License.

References

Banakh, V. A., Zapryagaev, V., Kavun, I., Sazanovich, V., and Tsvyk, R.: Experimental investigations of the variance and fluctuation spectra of intensity of a laser beam crossing the supersonic gas flow, Atmospheric and Oceanic Optics, 20, 368–373, 2007.

Best, G. and Hoffman, H.: The initial behavior of high altitude barium releases—I. The particulate ring, Journal of Atmospheric and Terrestrial Physics, 36, 1469–1473, https://doi.org/https://doi.org/10.1016/0021-9169(74)90225-6, 1974.

Chou, M.-Y., Shen, M.-H., Lin, C. C. H., Yue, J., Chen, C.-H., Liu, J.-Y., and Lin, J.-T.: Gigantic Circular Shock Acoustic Waves in the Ionosphere Triggered by the Launch of FORMOSAT-5 Satellite, Space Weather, 16, 172–184, https://doi.org/https://doi.org/10.1002/2017SW001738, 2018.

Emmert, J. T., Drob, D. P., Picone, J. M., Siskind, D. E., Jones Jr., M., Mlynczak, M. G., Bernath, P. F., Chu, X., Doornbos, E., Funke, B., Goncharenko, L. P., Hervig, M. E., Schwartz, M. J., Sheese, P. E., Vargas, F., Williams, B. P., and Yuan, T.: NRLMSIS 2.0: A Whole-Atmosphere Empirical Model of Temperature and Neutral Species Densities, Earth and Space Science, 8, e2020EA001 321, https://doi.org/https://doi.org/10.1029/2020EA001321, e2020EA001321 2020EA001321, 2021.

Fahleson, U., Fälthammar, C.-G., Pedersen, A., Knott, K., Brommundt, G., Schumann, G., Haerendel, G., and Rieger, E.: Simultaneous Electric Field Measurements Made in the Auroral Ionosphere by Using three Independent Techniques, Radio Science, 6, 233–245, https://doi.org/https://doi.org/10.1029/RS006i002p00233, 1971.

Föppl, H., Haerendel, G., Haser, L., Loidl, J., Lütjens, P., Lüst, R., Melzner, F., Meyer, B., Neuss, H., and Rieger, E.: Artificial strontium and barium clouds in the upper atmosphere, Planetary and Space Science, 15, 357–IN2, https://doi.org/https://doi.org/10.1016/0032-0633(67)90200-0, 1967.

Hedin, A. E.: Extension of the MSIS thermosphere model into the middle and lower atmosphere, J. Geophys. Res., 96, 1159–1172, 1991.

Jia, T.-M., Li, G.-X., Yu, Y.-S., and Xu, Y.-J.: Propagation characteristics of induced shock waves generated by diesel spray under ultra-high injection pressure, Fuel, 180, 521–528, https://doi.org/https://doi.org/10.1016/j.fuel.2016.04.009, 2016.

Kakinami, Y., Yamamoto, M., Chen, C.-H., Watanabe, S., Lin, C., Liu, J.-Y., and Habu, H.: Ionospheric disturbances induced by a missile launched from North Korea on 12 December 2012, Journal of Geophysical Research: Space Physics, 118, 5184–5189, https://doi.org/https://doi.org/10.1002/jgra.50508, 2013.

Landau, L. D. and Lifshitz, E. M.: Fluid Mechanics, Pergamon, Oxford, 1989.

Li, X., Xiong, B., Ding, F., Chen, G., Mao, T., and Song, Q.: Ionospheric Disturbances Excited by Launches of China's Long March 2C Rockets, Journal of Geophysical Research: Space Physics, 130, e2025JA033 845, https://doi.org/https://doi.org/10.1029/2025JA033845, e2025JA033845 2025JA033845, 2025.

Lin, C. H., Lin, J. T., Chen, C. H., Liu, J. Y., Sun, Y. Y., Kakinami, Y., Matsumura, M., Chen, W. H., Liu, H., and Rau, R. J.: Ionospheric shock waves triggered by rockets, Annales Geophysicae, 32, 1145–1152, https://doi.org/10.5194/angeo-32-1145-2014, 2014.

MacPhee, A. G., Tate, M. W., Powell, C. F., Yue, Y., Renzi, M. J., Ercan, A., Narayanan, S., Fontes, E., Walther, J., Schaller, J., Gruner, S. M., and Wang, J.: X-ray Imaging of Shock Waves Generated by High-Pressure Fuel Sprays, Science, 295, 1261–1263, https://doi.org/10.1126/science.1068149, 2002.

Merzkirch, W.: Flow Visualization, Academic Press, Inc., Orlando, second edn., 1987.

Rosenberg, N. W. and Best, G. T.: Chemistry of barium released at high altitudes, The Journal of Physical Chemistry, 75, 1412–1418, https://doi.org/10.1021/j100680a009, 1971.

https://doi.org/10.5194/egusphere-2026-2925
Preprint. Discussion started: 30 June 2026
© Author(s) 2026. CC BY 4.0 License.

Settles, G. S. and Hargather, M. J.: A review of recent developments in schlieren and shadowgraph techniques, Measurement Science and Technology, 28, 042 001, https://doi.org/10.1088/1361-6501/aa5748, 2017.

Taki, T., Sergienko, T., Brändström, U., Ogawa, Y., Nanjo, S., and Araújo, J.: Electric fields in and around an auroral arc and the inferred current system from the BROR sounding rocket experiment, EGUsphere, 2026, 1–19, https://doi.org/10.5194/egusphere-2026-1133, 2026.

Wang, J., Liu, S., Tao, S., Deng, X., Ye, Y., Meng, J., and Liu, Z.: High-precision measurement of refractive index in explosive-driven air blast waves for density and pressure determination, Journal of Applied Physics, 134, 124 501, https://doi.org/10.1063/5.0163533, 2023.

Wang, Y., song Yu, Y., xiu Li, G., and ming Jia, T.: Experimental investigation on the characteristics of supersonic fuel spray and configurations of induced shock waves, Scientific Reports, 7, 39 685, https://doi.org/10.1038/srep39685, 2017.

Wescott, E. M., Stolarik, J. D., and Heppner, J. P.: Electric fields in the vicinity of auroral forms from motions of barium vapor releases, Journal of Geophysical Research (1896-1977), 74, 3469–3487, https://doi.org/https://doi.org/10.1029/JA074i014p03469, 1969.

White, F. M.: Viscous Fluid Flow, McGraw-Hill, Inc., New York, 1991.

Yasyukevich, Y. V., Vesnin, A. M., Astafyeva, E., Maletckii, B. M., Lebedev, V. P., and Padokhin, A. M.: Supersonic Waves Generated by the 18 November 2023 Starship Flight and Explosions: Unexpected Northward Propagation and a Man-Made Non-chemical Depletion, Geophysical Research Letters, 51, e2024GL109 284, https://doi.org/https://doi.org/10.1029/2024GL109284, e2024GL109284 2024GL109284, 2024.